Supporting Information for

A Material Catalogue with Glass-Like Thermal Conductivity Mediated by the Crystallographic Occupancy for Thermoelectric Application

Zihang Liu[a], Wenhao Zhang[a,b], Weihong Gao[a] and Takao Mori[a,b*]

[a] WPI Center for Materials Nanoarchitectonics (WPI-MANA), National Institute for Materials Science (NIMS), Namiki 1-1, Tsukuba 305-0044, Japan

[b] Graduate School of Pure and Applied Sciences, University of Tsukuba, Tennodai 1-1-1, Tsukuba 305-8671, Japan

These authors contributed equally: Zihang Liu, Wenhao Zhang.

To whom correspondence should be addressed. E-mail: MORI.Takao@nims.go.jp

Materials and Methods

Synthesis

High-purity raw materials were directly weighed according to the nominal composition $Cu_{6-x}Ag_xTe_3S$ (x = 0, 1, and 2), Bi_5CuS_8 and Cr_5Te_8, transferred to the quartz tubes and sealed under high vacuum. These ampoules were put vertically into a programmable resistance box furnace, heated to 1373 K, held for 12 hours, slowly cooling down to 773 K, annealing for 7 days, and eventually quenched to room temperature in cold water. These obtained ingots were hand ground into fine powders and consolidated by spark plasma sintering (SPS, SPS-1080 System, SPS SYNTEX INC) under a pressure of 60 MPa under argon atmosphere. The sintering temperature for $Cu_{6-x}Ag_xTe_3S$, Bi_5CuS_8 and Cr_5Te_8 is about 723 K, 673 K, and 873 K, respectively.

Phase and property characterizations

The phase structure were characterized by powder X-ray diffraction (XRD, SmartLab3, Rigaku) with Cu K_α radiation and further analyzed by Rietveld refinement method using FullProf. Bar samples were cut from the pressed disks and used for simultaneous measurement of electrical resistivity (ρ) and Seebeck coefficient (S) on a commercial system (ULVAC ZEM-2). The thermal conductivity κ_{tot} was calculated using $\kappa_{tot} = DC_pd$, where D, C_p, and d are the thermal diffusivity, specific heat capacity, and density, respectively. The thermal diffusivity coefficient (D) and the specific heat capacity (C_p) were concurrently measured for the disk sample on a laser flash system (Netzsch LFA 467, Germany) with a pyroceram disk as a reference sample. The sample density (d) was determined by the Archimedes method. The low-temperature thermoelectric properties and heat capacity were measured using the PPMS (Physical Properties Measurement System, Quantum Design) with the thermal transport option (TTO) and heat capacity option, respectively. The microstructure and composition analysis were characterized using a field emission scanning electron microscope (FESEM, Hitachi S-4800) equipped with an energy dispersive spectrometer (EDS, Horiba EMAXEvolution X-Max). The room-temperature sound velocity measurement was performed by using a sing-around ultrasonic velocity measuring instrument Model

UVM-2, Ultrasonic Engineering Co.,Ltd. The simultaneous measurement of differential scanning calorimetry (DSC) and thermogravimetric (TG) was performed on a NETZSCH STA 449F1instrument under N_2 flow atmosphere, using a heating rate of 15 K/min.

REST-API method

In short, RESTful API is a common technique used in online databases and specifies the format of the query from users and replies from the online servers. In our case, a request is submitted to Crystallographic Open Database (COD) through python to ask for the information of compounds in the database, specifically, we impose criteria that 1) they should be binary or ternary compound; 2) contain one of the elements of S, Se, Te, and Sb; 3) do not contain 4f, 4d elements, and elements in period seven. The purpose of these criteria is to reduce the amount of compound returned that is of little interest for thermoelectricity (e.g., it excludes all the metal alloys).

The database server replies with a JSON file containing entries of the compounds, including cell parameters, space groups, journal reference as well as id number in the database that meet our criteria. To access the crystal structure of an individual compound, HTTP request is used to retrieve cif files from COD using the compound's id number, implemented in a python script.

Finally, all the cif files are processed using the PyCifRW library available in python. The structure is considered to contain partial occupancy if the _atom_site_occupancy field is less than 1. More detailed information can be found in the following website:

API usage: https://wiki.crystallography.net/RESTful_API/

Obtaining cif files: https://wiki.crystallography.net/howtoquerycod/

Computational methods

Taking account of the full effect of partial occupancy is beyond standard DFT calculation. Thus, a common way to treat partial occupancy in the calculation is to

generate a supercell that contains the possible configure by filling the partial occupancy site. However, for room temperature Cu_6Te_3S, its unit cell is already large, and it is computationally difficult to generate and treat its supercells. Thus, we only consider treating partial occupation in a unit cell (total 160 atoms in 180 crystallographic sites).

The partially occupied Cu are concentrated around the S atoms at the center of 1/8 cube (x,y,z = 1/4,1/4,1/4, and so on). 1) those separate "clusters" of partially occupied Cu do not interact with each other and 2) the number of Cu atoms in each of the clusters is approximately the total number of possible site times average partial occupancy. For example, in the cluster indicated by the red box, 9 crystallographic sites have an average occupancy of 0.6. Thus, we consider filling 5 atoms in those 9 crystallographic sites.

Finally, keeping the maximum crystal symmetry will generally speed up calculation by reducing the size of the irreducible Brillouin zone. We reduce the symmetry to $P2_12_12_1$ (19), which enables free arrangement inside a cluster but generates the same arrangement in the symmetry-related clusters. This means that now we only need to consider filling the atoms in one cluster and the other clusters will be filled by symmetry. However, it also means that the correlation of different clusters is not considered, since we assume that those clusters do not interact. Through the above consideration, the choice of filling the partially occupied site is dramatically decreased.

Among the structures generated by the above method, the one with the lower ground state energy will be the more like to appear and thus be more representative. We calculated the ground state energy for 40 configurations, and we choose 4 of them corresponding to the structure with the lowest ground state energy as input structures for the later phonon calculation. Phonon calculation shows that the 4 structures we use are both statically and dynamically stable. It should be also mentioned that the above method has its limitations, for example, it ignores the possible correlation between different clusters and does not guarantee that the structure calculated is representative under the experimental condition. However, it can greatly reduce the case we need to consider and produce structure representatives that allow us to investigate the reason for the associated low thermal conductivity.

Density functional theory (DFT) is used for the calculation of electronic structures and lattice dynamics. The calculation is performed using plane-waves implemented in the Quantum Espresso package[1] with projector augmented wave pseudopotentials[2] and

general gradient approximation (GGA) parameterized by Perdew, Burke and Ernzerhof's method (PBE) for the exchange and correlation functionals[3]. Spin-orbital coupling is not included in the calculation. We use the unit cell of 160 atoms in our calculation. The kinetic energy cutoff and the charge density cutoff are chosen to be 125 Ry and 750 Ry. Smearing with a parameter of 0.01 Ry is used for the Brillouin zone summation. For the electronic structure calculation, we use $3 \times 3 \times 3$ k grid while for the lattice dynamic calculation, we use Gamma-only calculation. The cell parameter is fixed at the experimental value of 16.69Å. For phonon calculation and the mode Gruneisen parameter, we use Phonopy package[4]. The atomic displacement of 0.05Å to extract the second-order force constant.

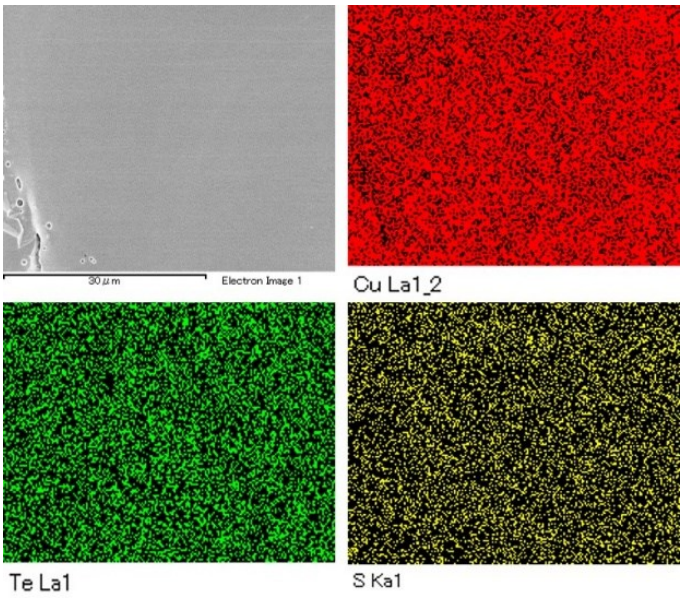

Figure S1. The scanning electron microscopy (SEM) energy dispersive spectrometer (EDS) composition mapping result of Cu_6Te_3S

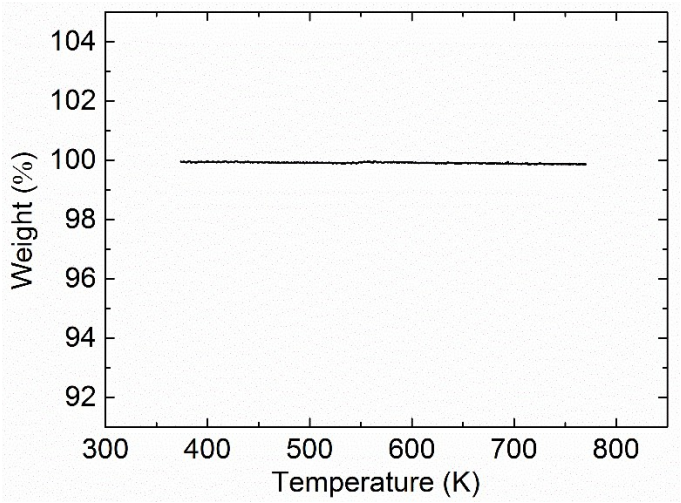

Figure S2. Thermogravimetry measurement result of the synthesized Cu_6Te_3S ingot

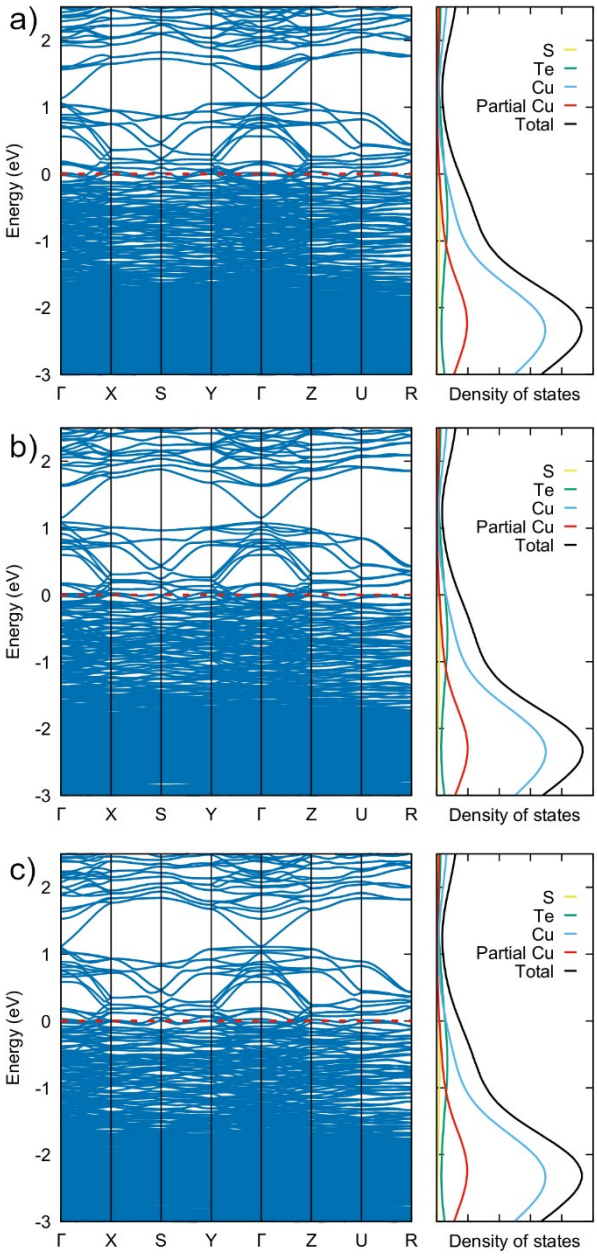

Figure S3. The calculated electronic band structure for the other three configurations of Cu_6Te_3S not shown in the main article

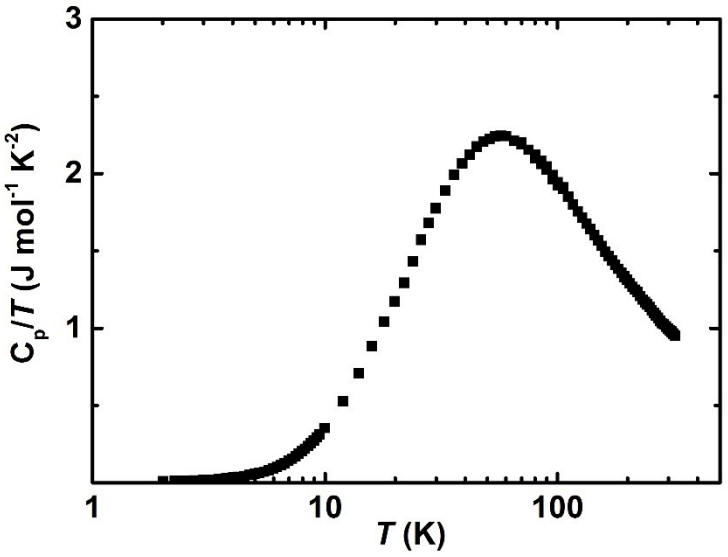

Figure S4. The low-temperature heat capacity C_p result of Cu_6Te_3S

Table S1. The obtained fitting parameter in the Debye-Einstein model

Model	δ J mol^{-1} K^{-2}	β J mol^{-1} K^{-4}	A1	Θ_{E1} K	A2	Θ_{E2} K
Debye + 1 E	0.0057	0.00187	17.01	58.2		
Debye + 2 E	0.00931	0.00106	33.87	74.41	4.13	39.01

Table S2. The obtained fitting parameter in the Debye-3Einstein model

`	β J mol^{-1} K^{-4}	A1	Θ_{E1} K	A2	Θ_{E2} K	A3	Θ_{E3} K
0.01019	0.00065	64.50	93.28	0.64	21.63	14.39	49.87

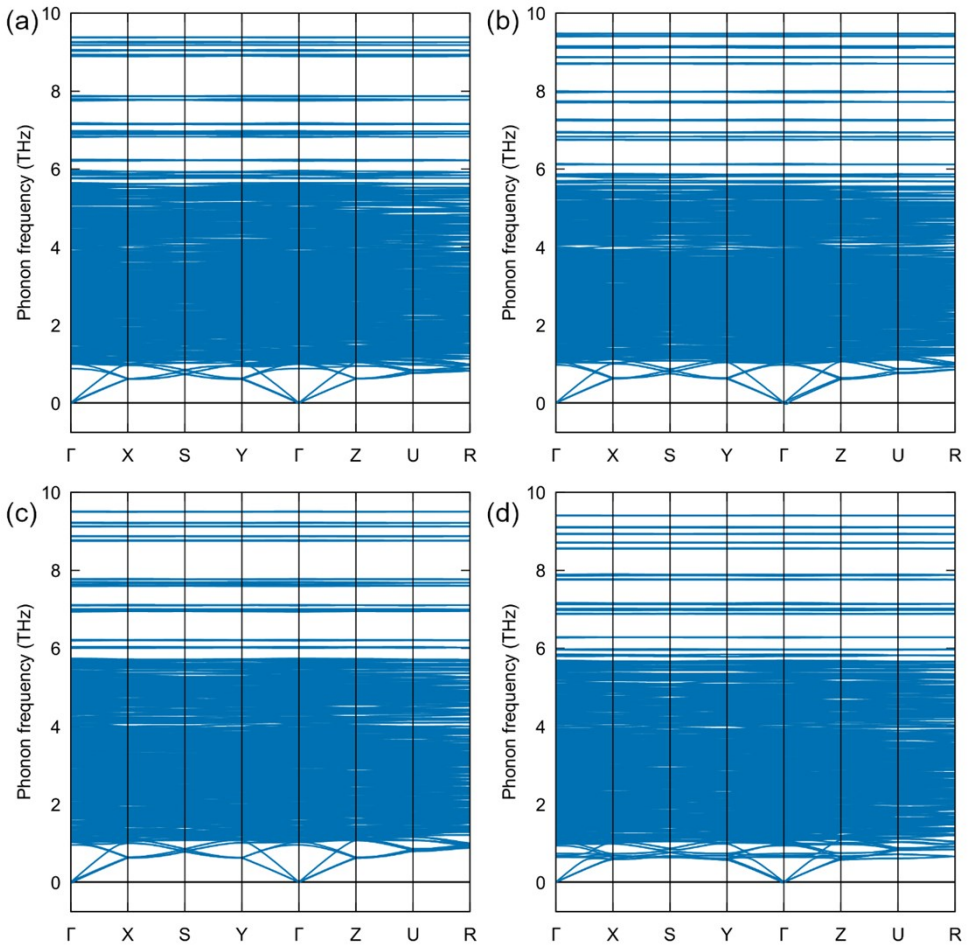

Figure S5. The calculated phonon dispersion for four configurations of Cu_6Te_3S

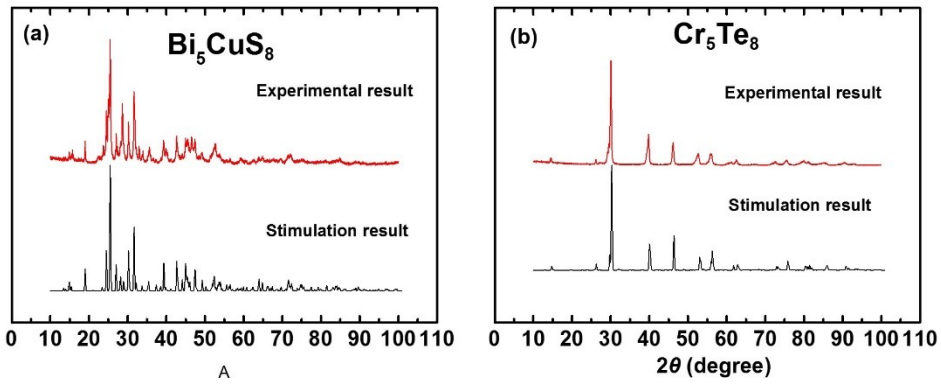

Figure S6. (a) and (b) XRD pattern of Bi_5CuS_8 and Cr_5Te_8, respectively

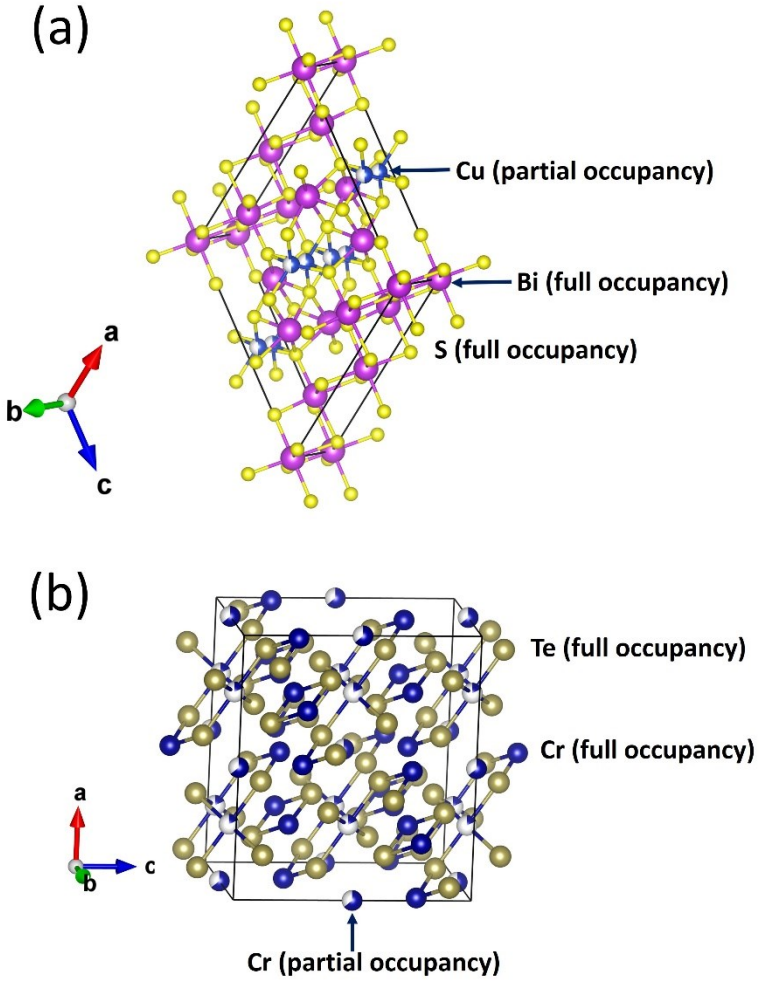

Figure S7. The crystal structure of Bi_5CuS_8 and Cr_5Te_8

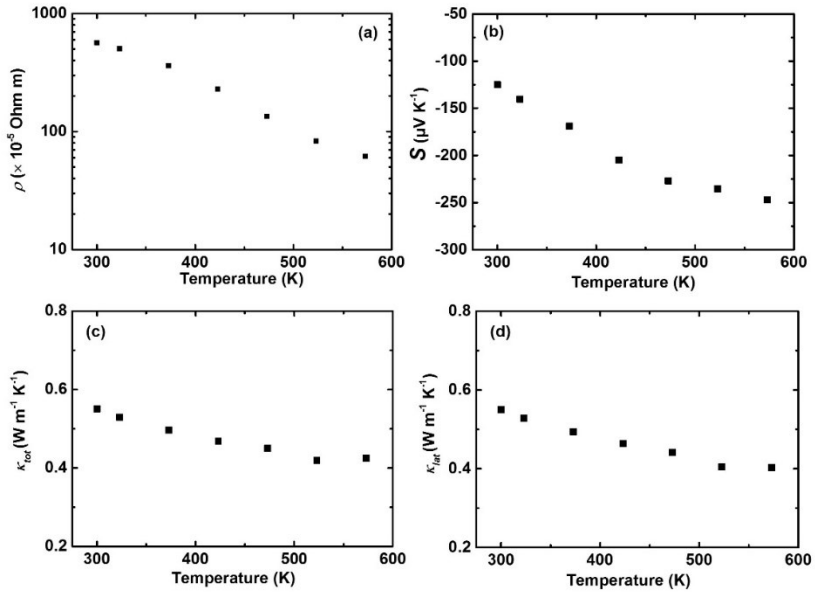

Figure S8. Temperature-dependent thermoelectric properties of Bi_5CuS_8.
(a)-(d) Electrical resistivity ρ, Seebeck coefficient S, total thermal conductivity κ_{tot}, and lattice thermal conductivity κ_{lat}.

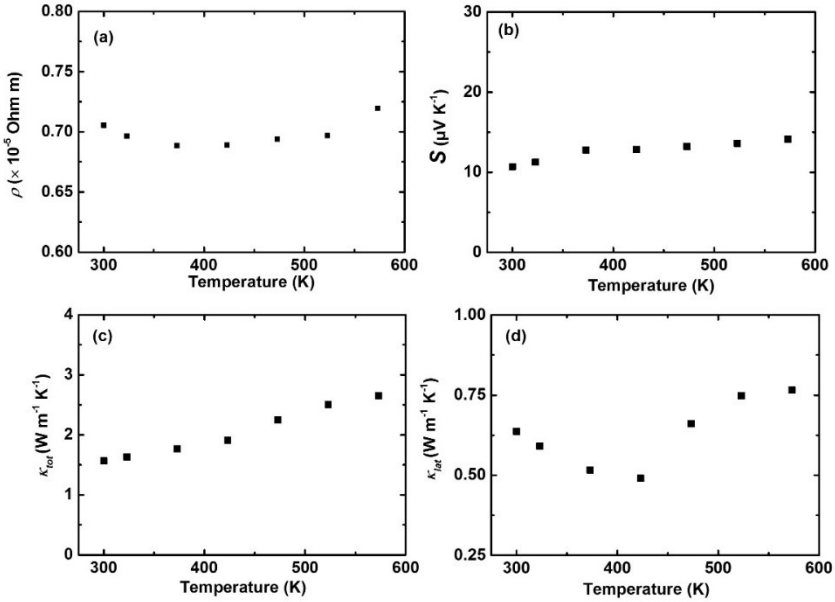

Figure S9. Temperature-dependent thermoelectric properties of Cr_5Te_8.
(a)-(d) Electrical resistivity ρ, Seebeck coefficient S, total thermal conductivity κ_{tot}, and lattice thermal conductivity κ_{lat}.

Table S3. Density data of Cu_6Te_3S, Bi_5CuS_8, and Cr_5Te_8

Sample composition	Theoretical density (g cm^{-3})	Measured density (g cm^{-3})	Relative density
Cu_6Te_3S	6.66	6.60	99.1%
Bi_5CuS_8	6.71	6.70	99.8%
Cr_5Te_8	6.67	6.50	97.5%

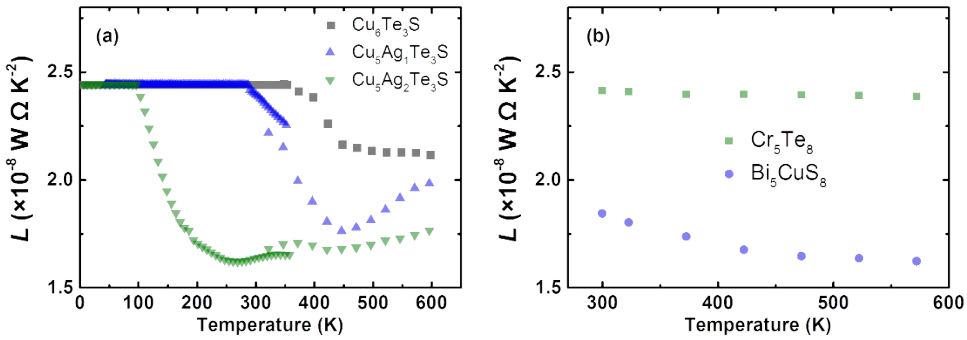

Figure S10. The calculated Lorenz number of $Cu_{6-x}Ag_xTe_3S$, Cr_5Te_8, and Bi_5CuS_8. The Lorenz number L was roughly calculated based on the following equation when $|S| > 10$ μ V K^{-1}.

$$L = 1.5 + \exp\left[-\frac{|S|}{116}\right]$$

where S is the measured Seebeck coefficient. For $|S| < 10$ μ V K^{-1}, we directly used the degenerate limit (2.44 × 10^{-8} W Ω K^{-2}) due to the ineffectiveness of these physical models.[5]

Table S4. The composition, mass per atom (M), and unit cell volume (V) of these common semiconductors and Zintl compounds, as well as compounds with partial occupancy[6-8]

Composition	M ($g\ mol^{-1}$)	V-unit cell volume ($Å^3$)	κ_{lat} ($W\ m^{-1}\ K^{-1}$)
Si	28.085	160.191	156
Ge	72.63	181.12	60
SiC	20	82.86	490
Se	78.97	94.72	4.5
Te	127.6	105.094	2.3
BN	12.405	47.28	391
BP	20.892	93.471	360
AlN	20.52	48.1895	319
AlP	28.978	163.088	90
AlAs	50.952	181.455	91
AlSb	74.371	230.967	56
GaN	41.865	52.804	130
GaP	50.3485	161.932	100
GaAs	72.322	180.761	44
GaSb	95.74	226.5269	33
$CuGaSe_2$	72.79	120.9516	12.9
$CuGaTe_2$	97.1	429.48	6.7
$CuInTe_2$	108.39	469.77	6
$AgInTe_2$	119.5	520.532	2.3
Mg_2Si	25.565	254.6	4
Mg_2Ge	40.413	262.284	6
Mg_2Sn	55.76	309.19	6
Cu_2GeSe_3	72.77	343.17	2.4
Cu_2GeTe_3	97.06	371.3	13
Cu_2SnTe_3	101.83	226.31	14.4
Cu_3AsS_4	49.175	292.853	3.2
Cu_3AsSe_4	72.64	166.375	2.5
Cu_3SbSe_4	78.51	391.155	1.5
GeTe	100.115	214.276	3
PbTe	167.4	269.836	2
SnTe	123.155	253	2.8
PbS	118.6	209.16	2.5
PbSe	143.085	229.67	1.6
SnSe	98.835	216.21	0.7
Bi_2Te_3	160.16	507.8	1.3
Bi_2S_3	102.8	527.166	1.5

Bi_2Se_3	131	421.73	2
$CoSb_3$	110.45	737.2	10
Ca_3AlSb_3	75.86	822.9	1.6
Sr_3GaSb_3	102.185	1884.1	1.2
$Yb_{11}InSb_9$	148.3	1247.117	0.8
$CaZn_2Sb_2$	85.04	126.85	2.6
$YbZn_2Sb_2$	111.81	126.15	4.3
$Yb_{14}MnSb_9$	146.78	6074.5	0.7
$Bi_4Cu_4Se_9$	106.0588235	1643.420347	0.3
Bi_5CuS_8	97.5	675.685503	0.55
Cr_5Te_8	98.76923077	1275.684	0.64
$GeSb_4Te_7$	121.07	369.237195	1.2
$Ba_2Sb_2Se_5$	101.45	1075	0.45
Ag_8GeTe_6	113.54	1159.387	0.25
Zn_8Sb_7	91.69	1480.6	0.33
Cu_2SnSe_4	80.24	183.696002	0.6
$Ba_8Ga_{16}Ge_{30}$	81.74	1244.031159	1.2
$Cu_4Sn_7S_{16}$	59.19	1694.823	1.1
Cu_5FeS_4	50.18	1323.97	0.4
Cu_6Te_3S	79.61	3176.07	0.3

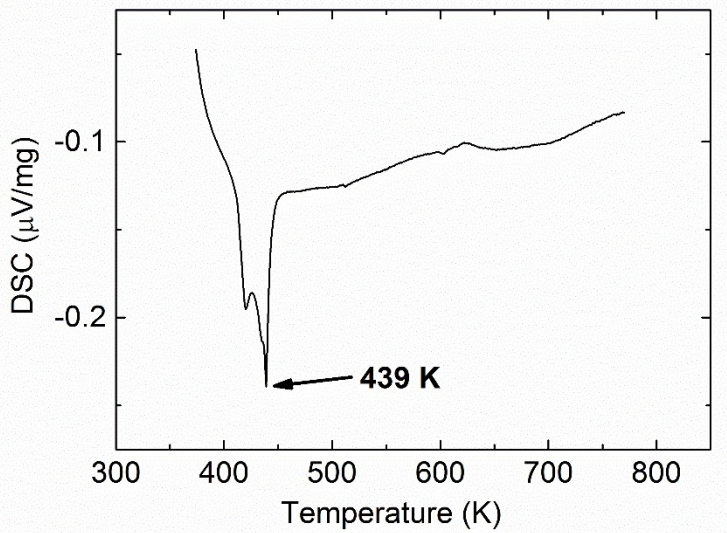

Figure S11. DSC measurement result of undoped Cu_6Te_3S

References

1. P. Giannozzi, *J. Phys. Condens. Matter*, 2009, **21**, 395502-395520(395519).
2. P. E. Blöchl, *Phys. Rev. B*, 1994, **50**, 17953.
3. J. P. Perdew, K. Burke and M. Ernzerhof, *Phys. Rev. Lett.*, 1996, **77**, 3865.
4. A. Togo and I. Tanaka, *Scr. Mater.*, 2015, **108**, 1-5.
5. H.-S. Kim, Z. M. Gibbs, Y. Tang, H. Wang and G. J. Snyder, *APL Materials*, 2015, **3**, 041506.
6. O. Madelung, *Semiconductors: Data Handbook*, Springer Berlin Heidelberg, New York, 2004.
7. S. Q. Lin, W. Li, S. S. Li, X. Y. Zhang, Z. W. Chen, Y. D. Xu, Y. Chen and Y. Z. Pei, *Joule*, 2017, **1**, 816-830.
8. E. S. Toberer, A. F. May and G. J. Snyder, *Chem. Mater.*, 2009, **22**, 624-634.